

Proton irradiation induced defects in β - Ga_2O_3 : A combined EPR and theory study

Cite as: APL Mater. 7, 022521 (2019); <https://doi.org/10.1063/1.5053158>

Submitted: 22 August 2018 . Accepted: 16 December 2018 . Published Online: 22 January 2019

Hans Jürgen von Bardeleben , Shengqiang Zhou , Uwe Gerstmann, Dmitry Skachkov , Walter R. L. Lambrecht, Quoc Duy Ho, and Peter Deák

COLLECTIONS

Paper published as part of the special topic on [Wide Bandgap Oxides](#)



View Online



Export Citation



CrossMark

ARTICLES YOU MAY BE INTERESTED IN

[Deep acceptors and their diffusion in \$\text{Ga}_2\text{O}_3\$](#)

APL Materials 7, 022519 (2019); <https://doi.org/10.1063/1.5063807>

[Impact of proton irradiation on conductivity and deep level defects in \$\beta\$ - \$\text{Ga}_2\text{O}_3\$](#)

APL Materials 7, 022510 (2019); <https://doi.org/10.1063/1.5054826>

[Impact of deep level defects induced by high energy neutron radiation in \$\beta\$ - \$\text{Ga}_2\text{O}_3\$](#)

APL Materials 7, 022502 (2019); <https://doi.org/10.1063/1.5054606>

additive manufacturing epitaxial crystal growth cerium oxide polishing powder silver nanoparticles sputtering targets III-IV semiconductors CVD precursors europium phosphors

AMERICAN ELEMENTS
THE ADVANCED MATERIALS MANUFACTURER®

deposition slugs OLED Lighting spintronics solar energy osmium nanoribbons thin films chalcogenides AuNPs GDC Li-ion battery electrolytes 99.999% ruthenium spheres

endoheral fullerenes copper nanoparticles diamond micropowder CIGS MBE grade materials palladium catalysts flexible electronics beta-barium borate borosilicate glass dysprosium pellets YBCO pyrolytic graphite 3d graphene foam indium tin oxide mesoporous silica raman substrates sapphire windows tungsten carbide InGaAs barium fluoride carbon nanotubes lithium niobate scandium powder

gallium lump glassy carbon nanodispersions InAs wafers laser crystals ultra high purity materials MOFs surface functionalized nanoparticles organometallics quantum dot Al Si P S Cl Ar rare earth metals photovoltaics refractory metals MOCVD superconductors transparent ceramics ultra high purity silicon

American Elements opens up a world of possibilities so you can **Now Invent!**

Over 15,000 certified high purity laboratory chemicals, metals, & advanced materials and a state-of-the-art Research Center. Printable GHS-compliant Safety Data Sheets. Thousands of new products. And much more. All on a secure multi-language "Mobile Responsive" platform.

perovskite crystals yttrium iron garnet alternative energy h-BN gold nanocubes graphene oxide macromolecules photonics rhodium sponge fiber optics beamsplitters infrared dyes zeolites fused quartz metallocenes platinum ink buckyballs Ti-6Al-4V

Now Invent.™
The Next Generation of Material Science Catalogs

www.americanelements.com

Proton irradiation induced defects in β -Ga₂O₃: A combined EPR and theory study

Cite as: APL Mater. 7, 022521 (2019); doi: 10.1063/1.5053158
Submitted: 22 August 2018 • Accepted: 16 December 2018 •
Published Online: 22 January 2019



Hans Jürgen von Bardeleben,¹  Shengqiang Zhou,²  Uwe Gerstmann,³ Dmitry Skachkov,⁴ 
Walter R. L. Lambrecht,⁴ Quoc Duy Ho,⁵ and Peter Deák⁵

AFFILIATIONS

¹Sorbonne Université, Institut des Nanosciences de Paris, UMR7588 au CNRS, 4 Place Jussieu, 75005 Paris, France

²Helmholtz Zentrum Dresden Rossendorf, Institute of Ion Beam Physics and Materials Research, Bautzner Landstrasse 400, D-013128 Dresden, Germany

³Lehrstuhl für Theoretische Physik, Universität Paderborn, 33098 Paderborn, Germany

⁴Department of Physics, Case Western Reserve University, 10900 Euclid Avenue, Cleveland, Ohio 44106-7079, USA

⁵Bremen Center for Computational Materials Science, University of Bremen, P.O. Box 330440, D-28334 Bremen, Germany

ABSTRACT

Proton irradiation of both n-type and semi-insulating bulk samples of β -Ga₂O₃ leads to the formation of two paramagnetic defects with spin $S = 1/2$ and monoclinic point symmetry. Their high introduction rates indicate them to be primary irradiation induced defects. The first electron spin resonance (EPR1) has a g-tensor with principal values of $g_b = 2.0313$, $g_c = 2.0079$, and $g_a = 2.0025$ and quasi-isotropic superhyperfine interaction of 13G with two equivalent Ga neighbors. Under low temperature photoexcitation, this defect is quenched and replaced by a different metastable spin $S = 1/2$ center of comparable intensity. This second defect (EPR2) has similar principal g-values of $g_b = 2.0064$, $g_c = 2.0464$, and $g_a = 2.0024$ and shows equally superhyperfine interaction with two equivalent Ga atoms. This EPR2 defect is stable up to $T = 100$ K, whereas for $T > 100$ K the initial defect is recovered. Density functional theory calculations of the spin Hamiltonian parameters of various intrinsic defects are carried out using the gauge including projector augmented wave method in order to determine the microscopic structure of these defects. The intuitive models of undistorted gallium monovacancies or self-trapped hole centers are not compatible with neither of these two defects.

© 2019 Author(s). All article content, except where otherwise noted, is licensed under a Creative Commons Attribution (CC BY) license (<http://creativecommons.org/licenses/by/4.0/>). <https://doi.org/10.1063/1.5053158>

β -Ga₂O₃ is a wide bandgap (4.8 eV) semiconductor, which has been studied in the past by electron spin resonance (EPR) due to its interesting shallow donor properties. These early measurements, which were performed on non-intentionally doped n-type single crystals, concerned dynamic nuclear polarization and bistability effects.^{1,2} At that time, the shallow donor was believed to be related to oxygen vacancy defects but recent theoretical predictions do exclude this model.^{3,4} The EPR spectra of some 3d transition metals (Fe³⁺, Mn²⁺, Cr⁺, Ti³⁺) have equally been investigated.⁵⁻⁷ Recently β -Ga₂O₃ has attracted new interest due to its demonstrated applications in microelectronics and the availability of single crystals and epitaxial layers with controlled electronic properties. For a detailed review, see Ref. 8. Both bulk single crystals and

doped epitaxial layers can now be purchased commercially from different suppliers.

Intrinsic point defects in β -Ga₂O₃ have not yet been clearly identified. They are expected to occur as native defects due to non-stoichiometric growth conditions but can also be generated by irradiation with high energy particles. Very first EPR results of neutron irradiated,⁹ bulk samples have been published recently, and the model of an octahedral gallium monovacancy defect has been proposed tentatively. Gallium vacancy defects and oxygen vacancy defects have also been evoked before in different optical and electrical studies¹⁰⁻¹³ of irradiated samples, but the assignment to a microscopic model is in general not possible with those techniques. Very recently we have undertaken a detailed theoretical study¹⁴

of the electronic structure and spin properties of the main, vacancy and interstitial related, intrinsic point defects in β - Ga_2O_3 . The results obtained in Ref. 14 can be used to identify from their spin Hamiltonian parameters the paramagnetic defects observed by EPR. In this work, we present additional experimental results on proton irradiation induced defects in β - Ga_2O_3 .

β - Ga_2O_3 has a monoclinic crystal structure with space group $C2/m$ described by the three lattice vectors **a**, **b**, **c** and the angle β between **a** and **c**.¹⁵ This low symmetry structure gives rise to two nonequivalent gallium lattice sites and three nonequivalent oxygen lattice sites. Due to the different site symmetries, distorted octahedral and tetrahedral for the Ga sites and lower symmetry 3-fold and 4-fold bonded oxygen sites, a rather complicated situation can be expected for the case of vacancy related centers. In addition, as vacancy defects are expected to be deep centers, the Fermi level position is another key parameter, which determines their charge and spin states. In this wide bandgap material for most deep centers, more than one charge transition level will occur in the gap¹³ and thus their EPR signature will change with the electrical compensation. To be more specific, the two gallium vacancy defects ($V_{\text{Ga}}(\text{tetra})$ and $V_{\text{Ga}}(\text{octa})$) can take charge states from 0 to 3⁻; they are expected to be paramagnetic in the 2⁻, 1⁻, and 0 charge states with a spin $S = 1/2$, $S = 1$, and $S = 3/2$, respectively, and diamagnetic in the 3⁻ charge state (Fig. 1). Thus in n-type conductive samples, the V_{Ga} centers will not be observable by EPR. In Fe doped semi-insulating Ga_2O_3 , the Fermi level is lowered and if pinned by the 2⁺/3⁺ level, the tetrahedral V_{Ga} is expected to become EPR active, while the octahedral V_{Ga} is still in the diamagnetic 3⁻ charge state. The charge transition levels of the V_{Ga} centers were obtained from density functional theory (DFT) calculations,²² and the one for $\text{Fe}^{2+/3+}$ was obtained from deep level transient spectroscopy (DLTS).¹⁷

In this work, we present further EPR results of the paramagnetic defects introduced by high-energy proton irradiation

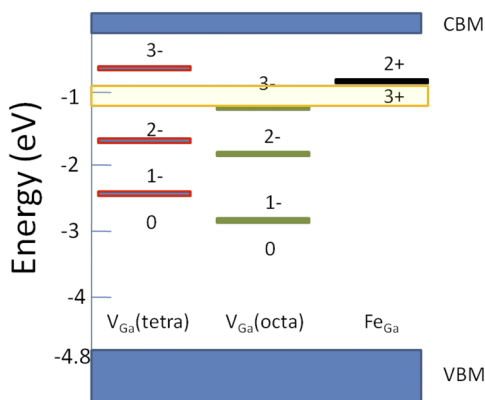


FIG. 1. Charge transition levels for the gallium vacancies and the Fe acceptor;^{14,17} the Fe 2⁺/3⁺ configurations correspond to the negatively charged and neutral acceptor states.

and in n-type and Fe doped bulk Ga_2O_3 and analyze different defect models based on their spin Hamiltonian parameters obtained by first principle calculations.

Our study was performed with commercially purchased (Tamura Corp.) (010) oriented β - Ga_2O_3 bulk samples of 400 μm thickness and $10 \times 15 \text{ mm}^2$ dimensions. The samples had been grown by the edge-defined film-fed (EFG) growth. Both non-intentionally doped n-type samples with a carrier concentration of $2 \times 10^{17} \text{ cm}^{-3}$ and Fe doped semi-insulating samples have been studied.

Both the initially n-type and the semi-insulating samples have been irradiated at room temperature with 12 MV protons to a fluence of 10^{16} cm^{-2} . SRIM simulations of the irradiation induced defect formation (Fig. 2) assuming displacement energies of 25 eV (Ga) and 28 eV (O) predict an introduction rate of the order of 500 cm^{-1} for both Ga and O vacancies and place the end of the range region outside the samples. Thus hydrogen related defects will not be considered in the following. As SRIM does not take into account the crystal structure, the displacement energies might also be different for the nonequivalent Ga and O lattice sites; thus SRIM simulations are expected to give order of magnitude values only.

The EPR measurements have been performed with a CW X-band spectrometer in the temperature range from $T = 4 \text{ K}$ to 300 K. The samples were measured under thermal equilibrium conditions and under *in situ* optical excitation with light sources in the visible or ultraviolet region.

Absolute spin concentrations were determined with a calibrated spin standard sample ($\text{Al}_2\text{O}_3:\text{Cr}$) purchased from the National Bureau of Standards.

The g-tensors and hyperfine interactions of the main intrinsic defects have been obtained by first principle calculations. The calculations were performed with 160 and 240 atom supercells. The structures were relaxed within a hybrid functional with 26% exact exchange and no screening of the

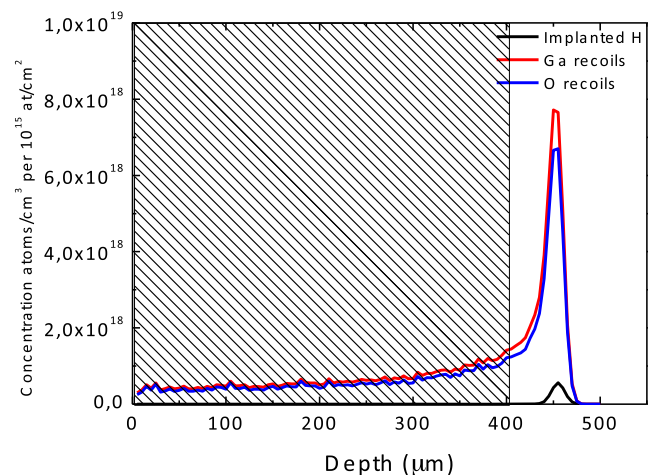


FIG. 2. Oxygen and gallium vacancy distribution as predicted by SRIM simulations assuming displacement energies of 25 eV for Gallium and 28 eV for oxygen atoms. Proton fluence: $1 \times 10^{15} \text{ cm}^{-2}$.

Coulomb interaction which was previously optimized.²² The EPR g -tensors were calculated using the Gauge Including Projector Augmented Wave Method (GIPAW) implemented as part of the Quantum Espresso package,²³ using the above relaxed structures but the electronic structure evaluated in the Perdew-Burke-Ernzerhof (PBE)-generalized gradient approximation (GGA)²⁴ because the GIPAW method does not yet include the possibility to include hybrid functional terms. The hyperfine tensors were calculated using the GGA+U method with the on-site Coulomb energy U on oxygen p -orbitals to increase the localization of the spin density on the oxygen and reduce it on the Ga second nearest neighbors to the defect. A reasonable value of $U = 4$ eV was chosen but appears to still overestimate the spread of the wave functions to the Ga. For more details of the calculation procedures, see Ref. 14.

We calculated, in particular, the gallium vacancy and oxygen interstitial related defects, which were considered to be the most probable candidates for the paramagnetic centers observed in our study.

Before irradiation, the n -type samples displayed at $T = 300$ K only the spin $S = 1/2$ EPR spectrum of a shallow donor (Fig. 3). The EPR spectrum of the shallow donor has been reported before.¹⁶ It is characterized by a spin $S = 1/2$ state, a monoclinic g -tensor, and a linewidth, which varies drastically with the donor concentration. In these bulk samples, the shallow donor is related to a contamination with Si, which is a substitutional defect on the tetrahedral gallium site. In the semi-insulating Fe doped samples, we observe two spin $S = 5/2$ spectra, which have already been attributed to Fe^{3+} impurities on the tetrahedral and octahedral gallium lattice sites. Fe is a gallium substituted defect, occupying both tetrahedral and octahedral Ga lattice sites.⁶ The spin Hamiltonian parameters of these centers have been reported before. Fe^{3+} on both lattice sites has a high spin $S = 5/2$ ground state and gives rise in X-band to allowed and forbidden transitions as

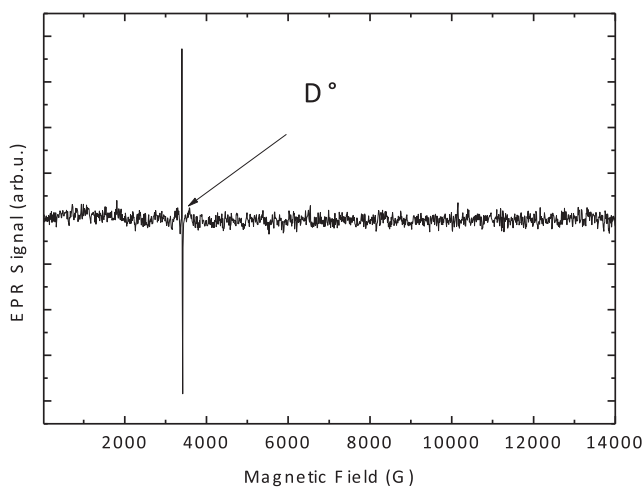


FIG. 3. Large scale EPR spectrum of the n -type sample before irradiation showing only the shallow donor resonance D° .

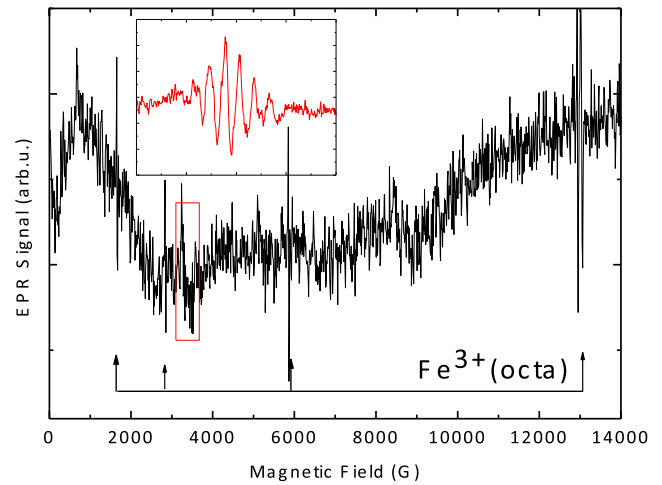


FIG. 4. Large scale EPR spectrum of the n -type sample after irradiation; the inset shows the EPR1 spectrum at higher resolution; B// \mathbf{b} .

the zero-field splitting parameter is of comparable magnitude to the Zeeman energy.

After the proton irradiation (Fig. 4), the initially n -type samples show no longer the shallow donor resonance, but we observe the multiline EPR spectrum of the $\text{Fe}^{3+}(\text{octa})$ center and an irradiation induced new spectrum with spin $S = 1/2$ (EPR1), which is the object of this study. As also previously observed,¹⁶ the proton irradiation has electrically compensated the n -type samples due to the introduction of deep acceptor centers.¹¹ This leads to a shift of the Fermi level toward midgap and converts the initially Fe^{2+} centers, which are EPR silent, into the $3+$ charge state. The observation of the Fe^{3+} spectrum is not unexpected as Fe is a common residual contamination of the bulk samples, introduced during the high temperature growth. More interestingly, the observation of the Fe^{3+} spectrum gives us an indication about the Fermi level position (Fig. 1) after the irradiation. It has recently been shown by DLTS measurements¹⁷ that the deep center E2 with an ionization energy of 0.78 eV, observed in bulk EFG samples, is associated with a Fe contamination and has been attributed to the $-/0$ level of the Fe acceptor. No distinction between $\text{Fe}^{3+}(\text{octa})$ and $\text{Fe}^{3+}(\text{tetra})$ has been made in that study. The proton irradiation has thus moved the Fermi level from the shallow donor position at $E_c - 0.04$ eV to below $E_c - 0.78$ eV.

In Fig. 5, we show a high-resolution spectrum of the EPR1 center for B// \mathbf{b} . The spectrum can be observed without a change in the spin Hamiltonian parameters between $T = 300$ K and 4 K. It is characterized by an electron spin $S = 1/2$, a monoclinic point symmetry, and an anisotropic g -tensor with principal axes parallel to the crystal \mathbf{b} , \mathbf{c} , and \mathbf{a}^* axes (Table I). It displays also a resolved hyperfine interaction with Ga neighboring atoms, giving rise to a seven line spectrum. The simulation of this very characteristic hyperfine structure shows that it is due to a superhyperfine interaction (SHF) with two equivalent Ga neighbors. It is the

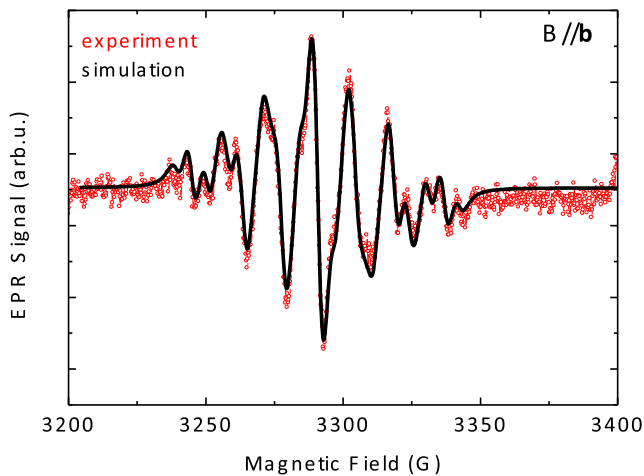


FIG. 5. Experimental EPR spectrum of the EPR1 center (red) and its simulation (black) with the SHF interaction with two equivalent Ga atoms; $B//b$.

presence of two Ga isotopes (^{69}Ga , ^{71}Ga) with different nuclear moments and different isotopic abundance, which gives rise to this very characteristic HF pattern (Fig. 6). Models assuming SHF interaction with 1, 3, or 4 equivalent Ga neighbors or multiple nonequivalent Ga neighbors are not compatible with the observed SHF structure. The HF interaction with oxygen— if present—is in general not observable due to the very low (0.038%) isotopic abundance of the isotope ^{17}O , which is the only oxygen isotope with a nuclear spin ($I = 5/2$); the main isotope ^{16}O has no nuclear spin. The principal values and principal axes of the g -tensor of this EPR spectrum have been determined from the angular variation of the EPR spectrum for a rotation of the applied magnetic field in three different lattice planes (Table I). The g -tensor is characterized by one g -value with a large deviation from the free electron value $-g_b = 2.0313$ — and two values close to the free electron g_c -value (Table I). Such a g -tensor is typical for hole centers on an oxygen p -orbital. This configuration of a hole on an oxygen p -orbital is the expected configuration of the Ga monovacancy defect.

The g -tensor anisotropy and principal values are similar to the case of the cation vacancies in ZnO, another wide

bandgap semiconductor. In the case of wurzite ZnO, the zinc vacancy in the $2-$ charge state, V_{Zn}^{2-} , is equally a spin $S = 1/2$ center with a hole localized on a first nearest neighbor oxygen atom.¹⁸ Due to the wurzite structure of ZnO, the c -axis aligned and the “in-plane” oxygen neighbors are not equivalent, and depending on which oxygen the hole is localized, two different centers have been observed. They are characterized by g -values of $g_{//c} = 2.0024$, $g_{lc} = 2.0193$ and $g_{xx} = 2.0173$, $g_{yy} = 2.0183$, $g_{zz} = 2.0028$ for the axial and basal configurations, respectively. These values are quite similar to those observed for the EPR1 defect and point clearly to a gallium vacancy related defect model. The situation in $\beta\text{-Ga}_2\text{O}_3$ is however more complex than in ZnO due to the lower symmetry of the Ga and O sites. In $\beta\text{-Ga}_2\text{O}_3$, even for an octahedral (tetrahedral) gallium monovacancy, the spin properties will depend on which of the nonequivalent first nearest neighbor oxygen atoms the p -hole is localized.

When studying radiation-induced defects in semiconductors, it is important to know, whether we deal with primary radiation induced centers or low intensity centers, which might have formed due to the presence of low temperature annealing stages. We have thus compared the concentration of the EPR1 center with those predicted by the SRIM modeling for primary defects. The spin concentration of the EPR1 center can be obtained by comparison with an Al_2O_3 :Cr spin standard sample by a double integration of their EPR spectra. We obtain for the EPR1 center a concentration of 10^{18} cm^{-3} , which is of the same order of magnitude as expected from the SRIM modeling for a primary defect (Fig. 2). We conclude thus that the EPR1 center is a primary defect.

After low temperature photoexcitation in the ultraviolet, the EPR1 spectrum is completely quenched and a new spin $S = 1/2$ EPR spectrum (EPR2) (Fig. 7) of comparable intensity but with different Spin Hamiltonian parameters is observed. The optical excitation has a threshold of 2.8 eV (Fig. 8). The spin Hamiltonian parameters of the EPR2 center are given in Table II. This center is equally characterized by an anisotropic g -tensor and a resolved SHF structure with two equivalent Ga neighbors. The principal values of the g -tensor and the SHF interaction parameter are of comparable magnitude to those of the EPR1 center. However, the principal axis of the highest g -value is now shifted to the c -axis.

In the Fe doped semi-insulating samples, we observe after proton irradiation the same EPR spectrum of the EPR1 center

TABLE I. Experimental and calculated EPR parameters for the EPR1 center and the undistorted $2-$ charged Ga monovacancies and the $V_{\text{Ga}}\text{-Ga}_i\text{-}V_{\text{Ga}}$ complex; S is the electron spin, O is the oxygen atom, on which the p -hole is localized, g is the principal g -value, N is the number of interacting Ga neighbors and their site symmetry, and A is the SHF interaction parameter; the experimental and computational uncertainties for the g and A values are also given. The values in boldface are experimental.

	Spin S	O atom	g_b	g_c	g_a	SHF N (Ga)	A (^{69}Ga) (G)
Experiment EPR1	1/2	...	2.0313 ± 0.0010	2.0079 ± 0.0010	2.0025 ± 0.0010	2	$13.8(\pm 0.5)$ $14.6(\pm 0.5)$ $12.8(\pm 0.5)$
Model V_{Ga}^{2-} (octa)	1/2	O(2)	2.0258 ± 0.005	2.0085 ± 0.001	2.0184 ± 0.001	2 Ga(tetra)	-22 ± 5
Model V_{Ga}^{2-} (tetra)	1/2	O(1)	2.0242	2.0068	2.0198	2 Ga(octa)	-22
V_{Ga} (tetra)- Ga_i - V_{Ga} (tetra)	1/2	O(1)	2.0251	2.0147	2.0048	2	-21

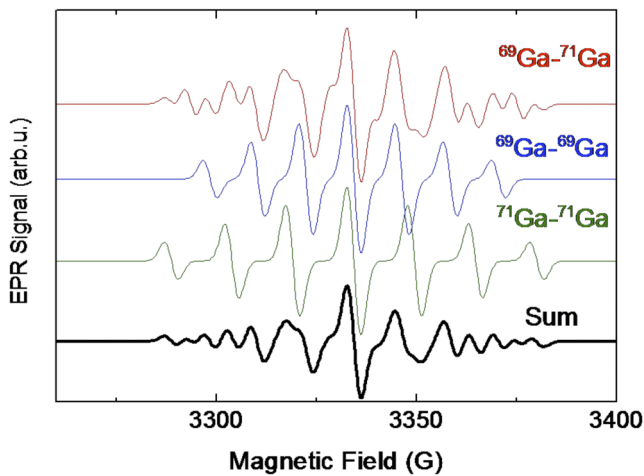


FIG. 6. Simulation of the EPR spectrum due to the SHF interaction with two equivalent Ga neighbors considering the presence of two Ga isotopes 69/71 with different nuclear moments and isotopic abundances.

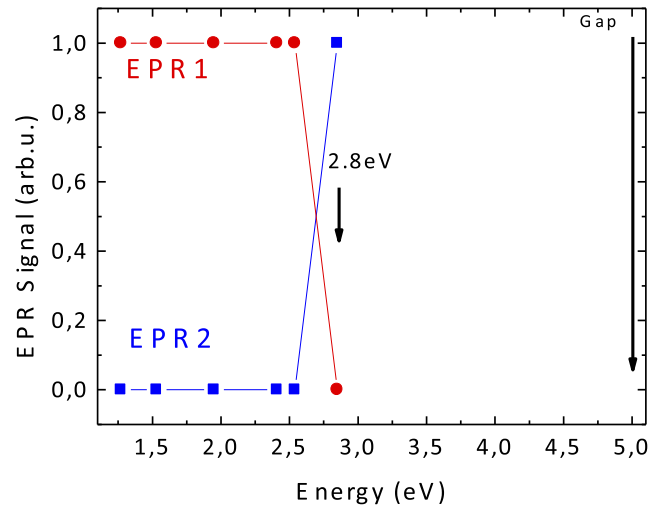


FIG. 8. Spectral dependence of the optically induced generation of the EPR2 spectrum and the quenching of the EPR1 spectrum.

as in the n-type samples. In addition, we observe simultaneously the two spectra of $\text{Fe}^{3+}(\text{octa})$ and $\text{Fe}^{3+}(\text{tetra})$. Under UV photoexcitation at temperatures below $T < 100$ K, the same transformation from the EPR1 to the EPR2 center is observed. The EPR2 center is metastable at low temperatures up to $T = 100$ K. For high temperatures, it is quenched and the original EPR1 spectrum is recovered (Fig. 8).

To interpret the photo-induced transformation from EPR1 to EPR 2, we have considered two models: (i) EPR2 is a metastable configuration of the EPR1 center, with a metastable state separated from the ground state by a barrier of the order of 0.1 eV, and (ii) the optical excitation induces a charge transfer from the EPR1 center to a second, different defect,

EPR2. If EPR1 and EPR2 are two different defects, their microscopic structure must be very similar as their spin Hamiltonian parameters are rather similar.

To assign these two centers to specific defect configurations, we have calculated the spin Hamiltonian parameters of different defect models. The highly anisotropic g -values of both centers EPR1 and EPR2 are characteristic for oxygen hole centers.^{14,18,19} The principal axis associated with the g -value close to 2.0023 indicates in the simple model of a p-hole the p-orbital orientation;^{18,19} within this model, the p-orbital is directed along the crystal \mathbf{a} -axis; it is not modified for the EPR2 center and stays parallel to the \mathbf{a} -axis for both centers. Only the principal axis associated with the highest g -values is now switched from \mathbf{b} to \mathbf{c} -axis. The SHF interaction of the EPR2 center is slightly reduced but is still characterized by the interaction with two equivalent Ga neighbors.

Whereas the configuration of a p-hole is the one expected for Ga vacancies, *a priori*, an oxygen hole center configuration might also occur for interstitial oxygen centers, another primary radiation induced defect. We have thus considered this possibility also in our modeling. As has been shown in Ref. 14, the oxygen interstitial is not stable and is predicted to form an O_2^- center with an oxygen dumbbell structure.

Concerning the EPR1 center, in Table I, we compare the g -tensor of the EPR 1 center with those of the two gallium monovacancies, the most obvious defect models. Both vacancies have a spin $S = 1/2$ ground state in the 2- charge state and charge transition levels close to the Fe acceptor level (Fig. 1). Furthermore, both defects present a SHF interaction with two equivalent Ga neighbors (Figs. 9 and 10). The principal values g_b , g_c of the g -tensor for both $V_{\text{Ga}}(\text{tetra})$ and $V_{\text{Ga}}(\text{octa})$ are also compatible with the experimental ones of the EPR1 center; however, the g_a value, which is close to 2.002 experimentally, is considerably higher for both vacancies. Based on

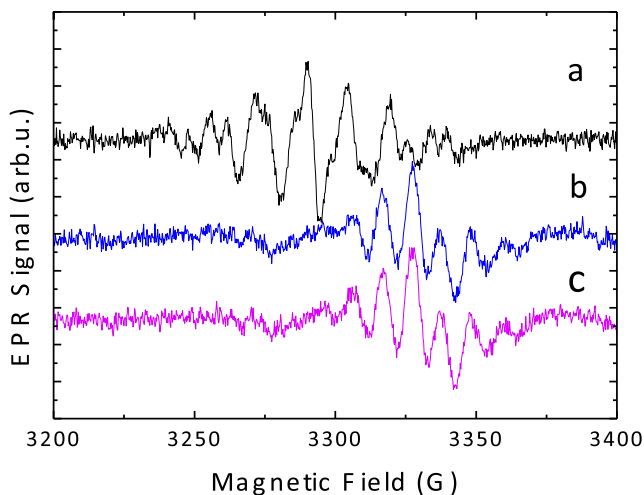


FIG. 7. EPR spectra before (a), under (b), and after (c) optical excitation with 2.8 eV; $T = 50$ K.

TABLE II. Experimental and calculated EPR parameters for the EPR2 center and the STH center, the O dumbbell, and a distorted octahedral Ga monovacancy; **S** is the electron spin, **O** is the oxygen atom on which the p-hole is localized, **g** is the principal g-value, **N** is the number of interacting Ga neighbors and their site symmetry, and **A** is the SHF interaction parameter; the experimental and computational uncertainties for the g and A values are also given. The values in boldface are experimental.

	Spin S	O atom	g_b	g_c	g_{a^*}	N (Ga)	A (^{69}Ga) (G)
Experiment	1/2		2.0064 \pm 0.0010	2.0464 \pm 0.0010	2.0024 \pm 0.0010	2	9.8 (\pm 0.5) 9.4 (\pm 0.5) 9.0 (\pm 0.5)
Model STH	1/2	O(1)	2.0228 \pm 0.005	2.0237 \pm 0.001	2.0113 \pm 0.001	2 1	-8 -16 \pm 5
$V_{\text{Ga}}(\text{oct})$ metastable	1/2	O(1)O(1)	2.0183	2.0372	2.0203	2 2	-16 -21
O ₂ - dumbbell	1/2	O(1) + O _i	2.0060	2.0306	2.0034	2 1	-8 -19

this discrepancy, these models for the EPR1 center will be discarded. Varley *et al.*²⁰ have recently shown that the isolated $V_{\text{Ga}}(\text{tetra})$ is not a stable configuration in $\beta\text{-Ga}_2\text{O}_3$ but transforms by a displacement of a lattice Ga atom into a $V_{\text{Ga}}(\text{tetra})\text{-Ga}_i\text{-}V_{\text{Ga}}(\text{tetra})$ complex. We have thus equally calculated the parameters for this defect. This defect (Fig. 11) has equally a spin $S = 1/2$ ground state and a g-tensor with principal axes aligned parallel to the crystal a^* , b , and c axes. The numerical values differ not much from those of the monovacancies, but this model predicts correctly a smallest principal g-value for the a^* -axis component. It fulfills also the other constraints of a SHF with two equivalent Ga neighbors. The absolute value of the SHF is still a factor of 2 too high for this model, just as for the vacancy models. It should be noted that this value depends very critically in the DFT+U calculations on computational parameters such as the Hubbard U value and might be thus overestimated. Another argument against the model of the $V_{\text{Ga}}(\text{octa})$ is the fact that it is expected to be in the 3- charge state (Fig. 1) for a Fermi level position pinned by the Fe acceptor. The tetrahedral vacancy and its lower energy complex are expected however to be in the EPR active state

in this case. We consider thus the model of a $V_{\text{Ga}}(\text{tetra})\text{-Ga}_i\text{-}V_{\text{Ga}}(\text{tetra})$ complex as the most plausible one for the EPR1 center.

Concerning the EPR2 center, as our calculations show no optically excited metastable state for the $V_{\text{Ga}}(\text{tetra})\text{-Ga}_i\text{-}V_{\text{Ga}}(\text{tetra})$ center, we conclude that the EPR2 center should be a different defect. Thus, its observation after photoexcitation must be due to a charge transfer process from the EPR1 center. As the EPR2 center is not observed in thermal equilibrium, it must have been in a different and diamagnetic charge state. The model of the $V_{\text{Ga}}(\text{octa})$ can be excluded as its g-tensor values are not compatible. We have thus considered additional defect models for the EPR2 center, which must reproduce the particular g-tensor properties. In particular, we investigated the properties of a metastable configuration of the octahedral Ga vacancy $V_{\text{Ga}}(\text{octa})'$ (Fig. 12), a self trapped

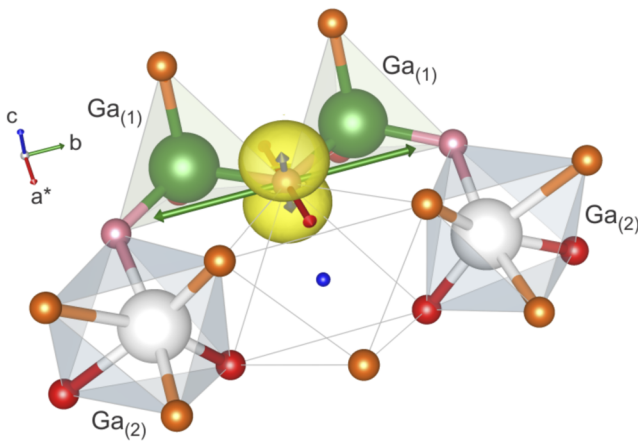


FIG. 9. $V_{\text{Ga}}^{2-}(\text{octa})$ local structure and spin density (yellow).

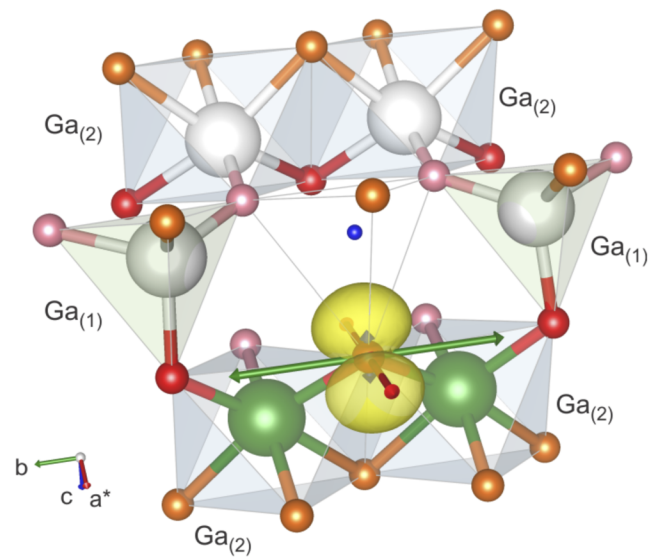


FIG. 10. $V_{\text{Ga}}^{2-}(\text{tetra})$ local structure and spin density (yellow).

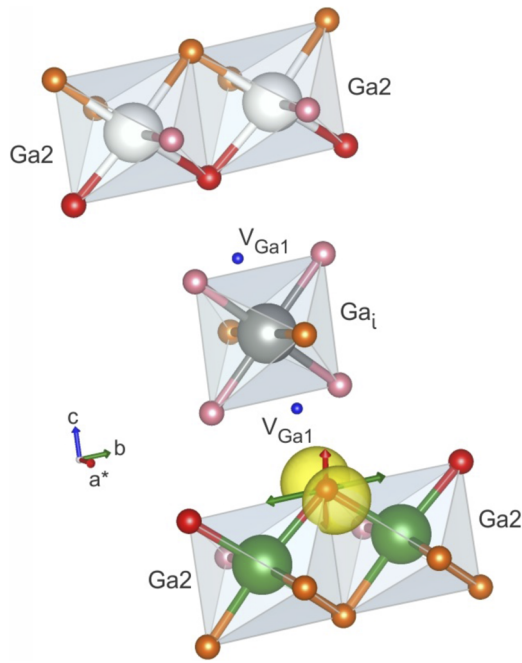


FIG. 11. $V_{\text{Ga}}(\text{tetra})\text{-Ga}_i\text{-}V_{\text{Ga}}(\text{tetra})$ local structure and spin density.

hole (STH) center, and an oxygen O_2 - dumbbell on an O(1) site. It should be noted that the EPR2 center has previously been observed and reported by Kananen *et al.*²¹ in neutron irradiated samples after low temperature X-ray excitation; these authors attributed this defect to a self-trapped hole center (STH) but without providing any modeling. Our calculations do not support this assignment, as the calculated g -values do not agree with the experimental findings (Table II), and more importantly, it would have hyperfine interaction with three Ga, which is incompatible with the observed SHF structure. Whereas the best agreement for the g -tensor is obtained for the oxygen dumbbell model, which reproduces nicely the

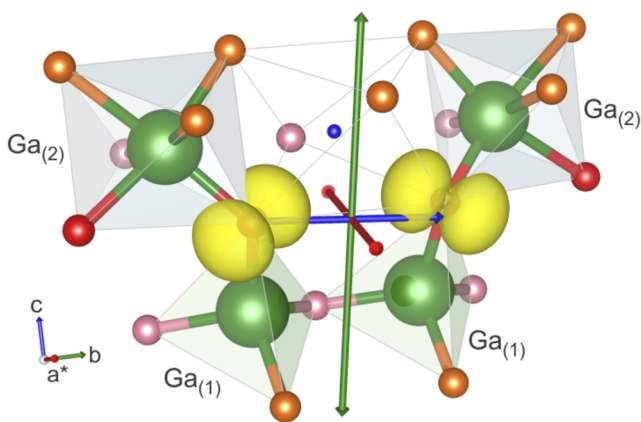


FIG. 12. $V_{\text{Ga}}^{2-}(\text{octa})$ metastable local structure and spin density (yellow).

g -tensor properties, the SHF interaction with $(2 + 1)$ Ga neighbors seems to exclude this model. Indeed, the simulation of the spectrum shape in the case of SHF interaction with three $(2 + 1)$ Ga neighbors changes the structure drastically and is not compatible with the experimental results. The principal characteristic of the g -tensor of the EPR2 center is the fact that the highest g -value is obtained for the component parallel to the c -axis. Such a configuration can be obtained for a tilted $V_{\text{Ga}}(\text{octa})$ configuration (Fig. 12), in which the oxygen atom, on which the hole is localized, is no longer in the mirror plane. This metastable octahedral model, which has tilted spins, still overestimates the smaller g -components and requires a SHF interaction with $(2 + 2)$ Ga neighbors. Nonetheless it is considered at present as a plausible model for the EPR2 center.

Proton irradiation introduces two main paramagnetic defects in $\beta\text{-Ga}_2\text{O}_3$, which are stable at room temperature. The high introduction rate shows them to be primary defect related. Their g -tensor properties are characteristic for oxygen hole centers, but their g -tensor values are not compatible with the model of an undistorted gallium monovacancy on a tetrahedral or an octahedral site (EPR1 center) or a self-trapped hole center (EPR2 center), as previously proposed.^{9,21} The tetrahedral vacancy on the other hand has a complex lowest energy $V_{\text{Ga}}(\text{tetra})\text{-Ga}_i\text{-}V_{\text{Ga}}(\text{tetra})$ configuration,²⁰ for which the g -tensor and SHF interaction agree well with the experimental ones for the EPR1 center. The models of an oxygen dumbbell and the metastable $V_{\text{Ga}}(\text{octa})$ configuration show only fair agreement with the EPR2 center parameters.

The work at CWRU was supported by the National Science Foundation under Grant No. DMR-1708593. The calculations were carried out at the Ohio Supercomputer Center. The work at BCCMS was supported by DFG Grant No. FR2833/63-1 and by the Supercomputer Center of Northern Germany (HLRN Grant No. hbc00027). U.G. acknowledges support from the Deutsche Forschungsgemeinschaft (DFG) priority Program No. SPP-1601. The ion irradiation was performed at the Ion Beam Center of Helmholtz-Zentrum Dresden-Rossendorf. The authors like to thank Sh. Akhmadaliev for his assistance with the proton irradiation.

REFERENCES

- E. Aubay and D. Gourier, *Phys. Rev. B* **47**, 15023 (1993).
- L. Binet and D. Gourier, *J. Phys. Chem.* **100**, 17630 (1996).
- Z. Hajnal *et al.*, *J. Appl. Phys.* **86**, 3792 (1999).
- J. B. Varley *et al.*, *Appl. Phys. Lett.* **97**, 142106 (2010).
- V. J. Folen, *Phys. Rev.* **139**, A1961 (1965).
- R. Büscher and G. Lehmann, *Z. Naturforsch.* **42a**, 67 (1986).
- F. Mentink-Vigier *et al.*, *Phys. Rev. B* **82**, 184414 (2010).
- S. J. Pearton *et al.*, *Appl. Phys. Rev.* **5**, 011301 (2018).
- B. E. Kananen *et al.*, *Appl. Phys. Lett.* **110**, 202104 (2017).
- S. Ahn *et al.*, *J. Vac. Sci. Technol. B* **34**, 041213 (2016).
- A. Y. Polyakov *et al.*, *Appl. Phys. Lett.* **112**, 032107 (2018).
- J. Yang and F. Ren, *J. Vac. Sci. Technol., B: Nanotechnol. Microelectron.: Mater., Process., Meas., Phenom.* **35**, 031208 (2017).
- H. Gao *et al.*, *Appl. Phys. Lett.* **112**, 242102 (2018).

- ¹⁴D. Skachkov *et al.*, e-print [arXiv:1808.00562](https://arxiv.org/abs/1808.00562) (2018).
- ¹⁵S. Geller, *J. Chem. Phys.* **33**, 676 (1960).
- ¹⁶M. Yamaga *et al.*, *Phys. Rev. B* **68**, 155207 (2003).
- ¹⁷M. E. Ingebrigtsen *et al.*, *Appl. Phys. Lett.* **112**, 042104 (2018).
- ¹⁸D. Galland and A. Hervé, *Phys. Lett. A* **33**, 1 (1970).
- ¹⁹L. E. Vanotti and J. R. Morton, *Phys. Rev.* **174**, 448 (1968).
- ²⁰J. B. Varley *et al.*, *J. Phys.: Condens. Matter* **23**, 334212 (2011).
- ²¹B. E. Kananen *et al.*, *J. Appl. Phys.* **122**, 215703 (2017).
- ²²P. Deak, Q. Duy Ho, F. Seemann, B. Aradi, M. Lorke, and T. Frauenheim, *Phys. Rev. B* **95**, 075208 (2017).
- ²³C. J. Pickard and F. Mauri, *Phys. Rev. Lett.* **88**, 086403 (2002).
- ²⁴J. P. Perdew, K. Burke, and M. Ernzerhof, *Phys. Rev. Lett.* **77**, 3865 (1996).